Johannes Claußnitzer[1]
Benjamin Bertleff[2]
Wolfgang Korth[1]
Jakob Albert[2]
Peter Wasserscheid[2]
Andreas Jess[1,*]

Kinetics of Triphase Extractive Oxidative Desulfurization of Benzothiophene with Molecular Oxygen Catalyzed by HPA-5

The triphasic aerobic extractive desulfurization of benzothiophene (BT) using an aqueous $H_8[PV_5Mo_7O_{40}]$ solution as catalyst and O_2 as oxidant was investigated. A time-resolved analysis of all reaction products in the gas, organic and aqueous phase, is given. The organic sulfur in BT is mainly converted to sulfuric acid. Mass transport limitations can be excluded. The reaction orders are 1 with regard to BT, and 0.5 both for HPA-5 and O_2. Calculated data derived from this mechanism with a power law kinetic approach show good agreement to the experimental data for conversions below 60 %. At higher BT conversions, significant deviations are found, suggesting that acidic products formed in the BT oxidation affect the catalyst and therefore the initial kinetics of the BT oxidation.

Keywords: Aerobic extractive oxidative desulfurization, Benzothiophene, Kinetic model, Polyoxometalates, Sulfate

Received: August 14, 2019; *revised:* October 08, 2019; *accepted:* December 17, 2019

DOI: 10.1002/ceat.201900448

This is an open access article under the terms of the Creative Commons Attribution License, which permits use, distribution and reproduction in any medium, provided the original work is properly cited.

Supporting Information available online

1 Introduction

Sulfur-free fuels can be produced from syngas (CO, H_2) by Fischer-Tropsch synthesis [1]. H_2 can be generated from various renewable resources, for example from water electrolysis [2], e.g., with surplus energy from renewable sources, or with enzymes from sugar as feedstock [3]. CO can be obtained by the reverse water-gas shift reaction of CO_2 and H_2 [4]. The production of fuels using the power-to-liquid (PtL) concept is technically feasible in an environmentally more benign way [5]. However, since production costs exceed those of conventional fuel production, PtL processes have not yet been established. Therefore, fuels from crude oil, supplied from the refinery industry, remain the main source for transportation and heating fuels.

Crude oil contains a vast number of different hydrocarbons (HCs) as well as considerable amounts of organic sulfur, nitrogen, and oxygen-containing compounds [6], which are regarded as the main impurities in terms of oil quality. The content of such elements depends on the oil well's geographical location [7]. If such compounds are burnt in combustion engines such as in cars or ships, sulfur dioxide (SO_2) or nitrogen oxides (NO_x) are emitted into the atmosphere as part of the exhaust gas stream [8]. Both oxides lead to acid rain, harming human health and the environment [9]. Furthermore, SO_2 is poisoning the catalytic converter of modern cars [10]. Within the EU, the S content in petrol and diesel fuel is currently limited to 10 ppmw [11], leading to a huge demand for deep-desulfurization techniques in the refining industry.

Since 1950, hydrodesulfurization (HDS) has been established as the main desulfurization technique in the refinery industry. Temperatures and H_2 pressures applied for desulfurization of gasoline are 310–370 °C and 30 bar, respectively. However, temperatures up to 400 °C and 100 bar are needed for desulfurization of diesel or heavier fuel oils [12]. The organic sulfur is hydrogenated yielding H_2S as the main product. As heterogeneous catalysts, alumina-supported CoMo or NiMo catalysts are used [13]. The H_2S is further processed downstream to elemental sulfur in the Claus process [14]. Sulfur can either be dumped or used for the production of sulfuric acid (SA) [15].

HDS is highly efficient in hydrogenating mercaptanes and disulfides, but benzothiophene (BT) and dibenzothiophene (DBT), especially alkylated BT or DBT compounds are, by orders of magnitude, less reactive, leading to even more severe reaction conditions as mentioned above. Under these harsh reaction conditions, unwanted side reactions, i.e., hydrogenation of aromatics or unsaturated HCs, do occur. As a result, hydrogen is wasted and the research octane number of gasoline is reduced [16]. In addition, high H_2 recycle streams are required, resulting in rather high investment as well as operational costs, making this process unsuitable for small and decentralized

[1]Johannes Claußnitzer, Dr. Wolfgang Korth, Prof. Dr.-Ing. Andreas Jess
jess@uni-bayreuth.de
Universität Bayreuth, Lehrstuhl für Chemische Verfahrenstechnik, Zentrum für Energietechnik (ZET), Universitaetsstrasse 30, 95447 Bayreuth, Germany.

[2]Benjamin Bertleff, Dr.-Ing. Jakob Albert, Prof. Dr. Peter Wasserscheid
Friedrich-Alexander-Universitaet Erlangen-Nuernberg, Lehrstuhl für Chemische Reaktionstechnik, Egerlandstrasse 3, 91058 Erlangen, Germany.

 © 2020 The Authors. Published by WILEY-VCH Verlag GmbH & Co. KGaA.

plants, e.g., for desulfurization units on container ships. To meet deep-desulfurization standards, alternative desulfurization methods are called for.

A promising alternative to HDS is oxidative desulfurization (ODS). In ODS, an oxidant is applied instead of hydrogen as reducing agent. Thus, H_2 is saved for other processes. Various oxidants have been published in the literature, leaving hydrogen peroxide (H_2O_2) as the most frequently used because of its high oxygen density, technical availability, and since water is formed as the only by-product [17]. Compared to H_2O_2, only few publications deal with O_2 or air as oxidant, although it is technically available, low-cost, and environmentally benign [18, 19]. The organic sulfur compounds are usually oxidized to their corresponding sulfones or sulfoxides [20], while increasing their polarity. Hereinafter, the sulfones as well as the sulfoxides can be removed by extraction with polar extraction agents such as acetonitrile, leading to extractive oxidative desulfurization (EODS).

Hirai et al. [21] oxidized dibenzothiophene in an aqueous biphasic non-catalytic photo-oxidation with O_2 or air as oxidant and a mercury lamp as light source to sulfuric acid, thereby combining oxidation and extraction to overcome the additional extraction step. This approach shows that aerobic extractive oxidative desulfurization (AEODS) is a promising alternative towards HDS and an improvement of EODS [22], since organic extracting agents are avoided. However, photolytic-driven oxidation seems until now not appropriate for an industrial application.

Polyoxometalates (POMs) have gained interest during the last decades as versatile oxidation catalysts for many reactions [23]. Among a wide variety of POMs, Keggin-POMs appear to be the most stable. In general, they are represented by the formula $[XM_{12}O_{40}]^{x-8}$, with the heteroatom X (X = P, Si etc.), the addenda atom M (M = Mo, W, V etc.) and x being the oxidation state [24]. There are several examples for the use of POM catalysts in desulfurization, either ODS or EODS [25]. Due to the oxidation potentials of sulfur-containing substrates, phosphovanadomolybdo heteropolyacids (PVMo-HPAs) such as $H_5[PV_2Mo_{10}O_{40}]$ can be used [26]. Khenkin et al. [27] demonstrated that this catalyst oxidizes different sulfides to the corresponding sulfoxides and sulfones under mild conditions, i.e., at around 70 °C and O_2 pressures up to 1 bar.

In a previous work, we presented an efficient way of oxidizing benzothiophene (BT) with $H_8[PV_5Mo_7O_{40}]$ (HPA-5) in an AEODS, yielding mainly sulfuric acid and other water-soluble sulfur-containing organic acids [28]. In order to design a technical reactor using molecular oxygen and an aqueous HPA-5 solution as catalyst, detailed knowledge of the kinetics of this oxidation reaction is mandatory. The aim of this work is to give a time-resolved analysis of all products in the gaseous, organic, and aqueous phase during desulfurization. By determining the partition coefficient K_n and the activation energy E_A, phase transition phenomena were taken into account, resulting in a simple power law kinetic model for the oxidation of BT in a batch process.

2 Experimental

2.1 Materials

All commercially available reagents were used without any further purification. The POM-catalyst HPA-5 ($H_8[PV_5Mo_7O_{40}]$), was synthesized according to literature [29]. Benzothiophene (Acros Organics, purity 97 %) and 2,2,4-trimethylpentane (Alfa Aesar, purity 99 %) were used as a standard model oil.

2.2 Experimental Setup and Catalytic Experiments

Desulfurization reactions were conducted in a 600-mL Hastelloy C276 autoclave equipped with a gas entrainment impeller, three valves to probe the organic, gaseous, and aqueous phase, and an inlet tube to control the O_2 pressure. The temperature was controlled with a heating jacket and an internal cooling coil. A typical experiment was carried out in the following manner: 0.5 mmol of the HPA-5 catalyst were dissolved in 200 mL deionized water ($c_{HPA\text{-}5}$ [1] = 2.5 mmol $L_{aq.}^{-1}$); 25 mmol of BT were dissolved in 100 mL of 2,2,4-trimethylpentane (c_{BT} = 250 mmol $L_{org.}^{-1}$, i.e., w_{BT} = 11 000 ppmw). This led to a molar sulfur-to-catalyst ratio of 50 and of 100, with regard to the concentration. Both solutions were charged into the reactor and the system was purged three times with O_2. While heating up to the reaction temperature, the solution was stirred with 50 min^{-1} to ensure isothermal conditions. To start the reaction, the pressure was set to 21 bar, leading to an O_2 pressure of about 17.5 bar (3.5 bar steam of water and 2,2,4-trimethylpentane). The impeller was set to 1000 min^{-1}. Samples of the three phases were taken in regular intervals.

2.3 Analytical Methods

To probe the organic and the aqueous phase, the impeller was set to 50 min^{-1} so that both phases can separate under isothermal conditions. In order to take a representative sample from each phase, a first sample was discarded from both phases. Afterwards a 5-mL sample of the aqueous and a 1-mL sample of the organic phase was taken and analyzed. The volume of each phase in the reactor at each time was calculated by weighing all samples taken from the vessel (see Supporting Information for details). Probes of the organic phase were diluted with 2,2,4-trimethylpentane. Total sulfur content was determined analytically with an N/S-analyzer from Antek Instruments. Sulfur compounds present in the organic phase were detected with a GC-PFPD (Varian CP 3800 with sulfur-sensitive detector, using a VF-5ht ultimetal 15 m × 0.32 mm ID0.10 µm DF column from Agilent (CP 9094)).

The aqueous phase was analyzed via inductively coupled plasma optical emission spectroscopy (ICP-OES) analysis (Perkin Elmer Plasma 400) for the total amount of sulfur and by ion chromatography (IC) for the detection of sulfuric acid

1) List of symbols at the end of the paper.

 © 2020 The Authors. Published by WILEY-VCH Verlag GmbH & Co. KGaA.

(SA), sulfoacetic acid (SAA), 2-sulfobenzoic acid (SBA) as well as formic acid (FA), acetic acid (AA), and oxalic acid (OA). IC was conducted on an ICS-3000 system (DIONEX) equipped with a conductivity detector using a GC11-HC/AS11-HC (2 mm×2.5 m) column set (DIONEX) and an AMMS300 (DIONEX) suppressor. For analyzing the catalyst, UV-VIS spectroscopy (Specord 200 Plus, Analytik Jena), Fourier transform infrared (FT-IR) spectroscopy (Nexus 470, Thermo Nicolet), and ^{31}P-NMR (Jeol ECX-400 MHz) were performed. Gaseous probes were taken with a 500-µL syringe. The probe subsequently was manually injected and analyzed using gas chromatography with a thermal conductivity detector (GC-TCD) for CO and CO_2.

Besides CO and CO_2, no further gaseous compounds were detected. By calibrating the GC-TCD for CO and CO_2, the partial pressure p_i (i = CO and CO_2) can be calculated. With vapor pressures for water [30] and 2,2,4-trimethylpentane [31] taken from literature, the partial pressure of oxygen was determined.

In order to obtain the molar mass of the catalyst, thermogravimetry (TG) analysis (TG/DTA 6300, Seiko Instruments) was carried out.

The yield Y_i of a sulfur-containing compound i was calculated with Eq. (1), where n_i is the sulfur amount of substance i and $n_{S,0}$ is the sulfur amount of the initially charged sulfur compound:

$$Y_i = \frac{n_i}{n_{S,0}} \tag{1}$$

The conversion X_{BT} of BT was calculated using Eq. (2), where $n_{BT,0}$ and $n_{BT,t}$ is the molar sulfur amount of BT at the beginning of the reaction and at running time t, respectively.

$$X_{BT} = \frac{n_{BT,0} - n_{BT,t}}{n_{BT,0}} \tag{2}$$

Since the progress of the desulfurization reaction is represented by the decrease of sulfur in the organic phase, the reaction rate r (Eq. (3)) is defined as the degradation rate of BT. The desulfurization reaction is a triphasic process. As the reaction takes place in the aqueous phase (Sect. 3.3), the reaction rate r is expressed with regard to the volume $V_{aq.}$ of the aqueous phase.

$$r = -\frac{1}{V_{aq.}} \frac{dn_{BT}}{dt} \tag{3}$$

3 Results and Discussion

3.1 Catalyst Synthesis and Characterization

The catalyst was prepared according to the synthesis method described by Odyakov et al. [29]. HPA-5 was characterized by ICP-OES, UV-Vis, FT-IR spectroscopy, thermogravimetry (TG), and ^{31}P-NMR spectroscopy (see Supporting Information Tab. S1 and Figs. S1–S4).

The molar ratio of vanadium to phosphorus and molybdenum to phosphorus within the HPA-5 structure was 5:1 and 7:1, respectively. ICP-OES measurements showed a molar ratio of 5.3:1 (V:P) and 7.2:1 (Mo:P), respectively, which is in satisfactory agreement with the theoretical values.

The UV-Vis spectrum of HPA-5 (Fig. S1) showed distinct absorption bands due to ligand-to-charge transfer (LMCT) absorptions of PMoV-HPAs: one absorption band at 202 nm (Mo–O) and two absorption bands at 321 nm and 369 nm (V–O) [32, 33].

Absorption bands described in literature for HPA-5 also appear in the IR spectrum (Fig. S2 and Tab. S1). These bands result in the interaction of P with O and Mo with O, respectively, whereby the interaction of Mo and O leads to three distinguishable bands, depending on the position of the oxygen within the Keggin structure [34].

In order to calculate the concentration of HPA-5 in the reactor, the molar mass M_{HPA-5} must be known. In Fig. S3, the thermogram of HPA-5 is depicted showing a two-step loss of water, typical for PVMo-HPAs [35]: 11.4 wt % loss of crystallization water and 5.1 wt % loss of constitutional water. This means that per mole HPA-5 17 moles of water are bound. Using this value, a molar mass of $M_{HPA-5} = 1910\ g\ mol^{-1}$ was calculated. The molar mass of the synthesized HPA-5 was constant over time, verified by repeated measurements.

^{31}P-NMR spectroscopy is a powerful method for analyzing PMoV-HPAs, since only one phosphorus atom is present within the Keggin structure. This P-atom interacts with the surrounding atoms, leading to distinct chemical shifts for the individual HPA-n (n = 0 to 5). In Fig. S4, a typical spectrum of HPA-5 is given, revealing that a solution of HPA-5 always contains the whole series of HPA-n from n = 1 to 5 and phosphoric acid, which is a residue from the synthesis. The number of peaks in the spectrum for every HPA-n corresponds with the number of isomers that is for HPA-1 ($H_4[PVMo_{11}O_{40}]$) only 1, for HPA-2 ($H_5[PV_2Mo_{10}O_{40}]$) 5, for HPA-3 ($H_6[PV_3Mo_9O_{40}]$) 13, and for HPA-4 ($H_7[PV_4Mo_8O_{40}]$) 27 isomers [36].

The experimental data confirmed that $H_8[PV_5Mo_7O_{40}]$ (HPA-5) was synthesized successfully.

3.2 Standard Oxidative Desulfurization Experiment and Mass Balance

The oxidative desulfurization of BT with HPA-5 is a triphasic process: HPA-5 homogeneously dissolved in the aqueous phase, BT homogeneously dissolved in 2,2,4-trimethylpentane and O_2 from the gaseous phase. To close the sulfur and carbon balance, all three phases must be taken into account. Fig. 1 presents a typical experiment with a total S content of $c_{BT} = c_S = 220\ mmol\ L_{org.}^{-1}$ (w_S = 11 000 ppmw). Typically, six samples were taken. Hence, a series of experiments under identical conditions were carried out to get sufficient data for the mass balance. The data given in Fig. 1 consists of four experiments conducted under identical conditions. They differ only in the time at which samples were taken: (1) t = 0–2.5 h, (2) t = 2.5–5 h, (3) t = 5–7.5 h, and (4) t = 7.5–17.5 h. Since probing was carried out in the organic and in the aqueous phase, the volume ratio $V_{aq}/V_{org.}$ was nearly constant for the whole experiment (Fig. S5).

 © 2020 The Authors. Published by WILEY-VCH Verlag GmbH & Co. KGaA.

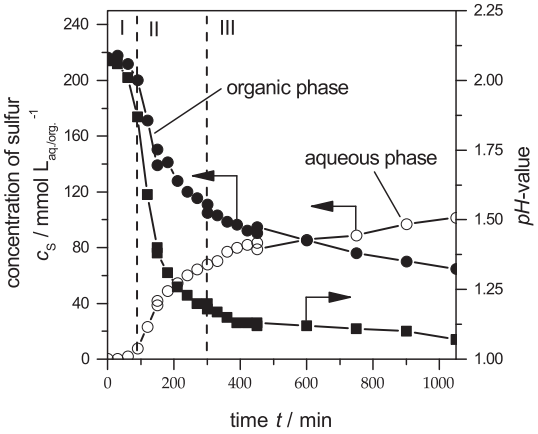

Figure 1. Concentration of BT in the organic ($c_{S,org.}$) and aqueous ($c_{S,aq.}$) phase and pH value of the aqueous phase during ODS with HPA-5 and O_2 as a function of time t. Conditions: $c_{BT,org.}(t=0)$ = 220 mmol $L_{org.}^{-1}$, $c_{HPA\text{-}5}$ = 2.30 mmol $L_{aq.}^{-1}$, T = 120 °C, p_{oxy} = 17.2 bar, n = 1000 min^{-1}.

The reaction can be divided into three different periods (Fig. 1). Period I is the induction period, in which the active catalyst species forms. Herein, the oxygen is not transferred via a Mars-van Krevelen mechanism from the HPA-5 Keggin anion, but via an O_2 molecule binding on or at least interacting with the anion of HPA-5 [37]. Since within the HPA-*n* structure the vanadium is mainly in the oxidation state +5, a certain amount of vanadium(V) within this structure must be reduced to vanadium(IV) to bind molecular oxygen, which takes up to 80 min, depending on the reaction conditions. In period II, the maximum reaction rate r is achieved. Finally, during period III, the reaction is inhibited by the products formed, leading to a decrease in the reaction rate r.

Corresponding to the decrease of the sulfur concentration in the organic phase (Fig. 1), the sulfur concentration in the aqueous phase increases with time. Since mainly water-soluble acidic products (Tab. 1) are formed, the pH-value of the aqueous solution decreases as the reaction proceeds (Fig. 1). Tab. 1 shows all sulfur-containing products analytically detected in the aqueous phase. No S-containing products were found in the organic phase at any time during the reaction, as indicated in Fig. S6. Hence, it can be assumed that benzothiophene reacts very fast to sulfur products soluble only in water, leading to an extractive oxidative desulfurization (EODS) process. It has to be noted that neither sulfones nor sulfoxides were detected analytically. Furthermore, only CO and CO_2, but no sulfur-containing products were found in the gaseous phase.

Figs. 2a and 2b illustrate the conversion X_{BT} of BT as well as the yields Y_i (with i = SA, SAA, and SBA; see also Tab. 1) for the sulfur-containing products in the aqueous phase as a function of time t for the experimental series presented in Fig. 1.

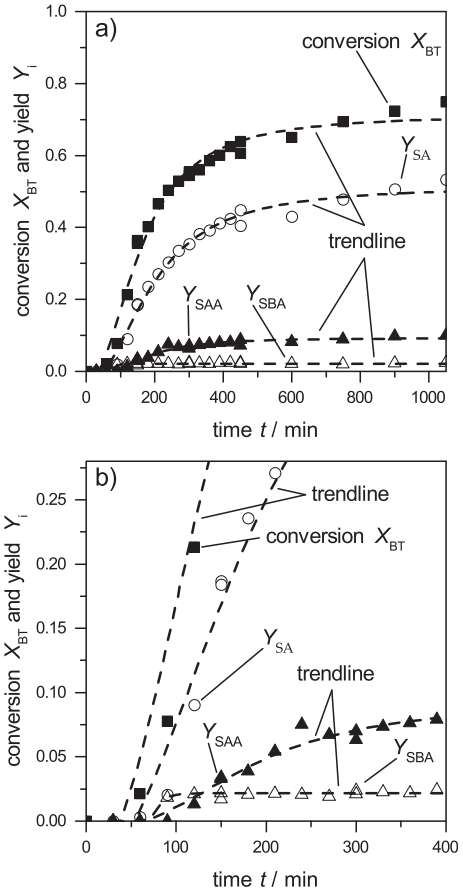

Figure 2. (a) Conversion X_{BT} of BT and yields Y_i for i = SA, SAA, and SBA as a function of time t for the standard experiment (see Fig. 1). (b) The same data with enlarged axis. For reaction conditions see Fig. 1.

Table 1. Sulfur-containing products of the desulfurization of BT with HPA-5 and O_2 found in the aqueous phase for the standard experiment (Fig. 1). Reaction conditions in Fig. 1.

Product	Yield Y_i after 90 min	Conversion X after 90 min	Yield Y_i after 210 min	Conversion X after 210 min
Sulfuric acid (SA)	0.02	0.08	0.27	0.47
Sulfoacetic acid (SAA)	0.00		0.05	
2-Sulfobenzoic acid (SBA)	0.02		0.02	

Following the induction period (I) of 70 min, ODS reaction (period II) starts and the conversion X_{BT} increases rapidly (Fig. 2b). Sulfuric acid is the first sulfur-containing product to appear. After 90 min, 2-sulfobenzoic acid emerges with nearly the same selectivity (Fig. S7b) as for H_2SO_4 at this time and with a yield of 0.02 (Fig. 2b), making SBA only a minor byproduct of the reaction. However, at the expense of the selectivity of SBA, the selectivity and the yield of sulfoacetic acid increases between 100 and 200 min reaction time. For a plot of the product concentration as a function of time t for SA, SAA, and SBA see Figs. S8a and S8b. The

 © 2020 The Authors. Published by WILEY-VCH Verlag GmbH & Co. KGaA.

yield of SBA is not increasing after 100 min (Fig. 2b), supporting our previously published mechanism that 2-sulfobenzoic acid is further oxidized to sulfoacetic acid which is subsequently oxidized to sulfuric acid [37].

After 200 min running time, the yields for SBA and for SAA remain constant (Fig. 2a), whereas the yield for sulfuric acid strongly rises until the reaction runs for 400 min. Thereafter, the yields for sulfuric acid grows linearly with the increase of the conversion, indicating that all sulfur is oxidized directly to SA. Both observations indicate a substantial decrease in catalyst activity. The change of reactivity correlates with the pH-value; here, the initial pH of 2.2 is dropping below 1.1 as the reaction proceeds, as demonstrated in Fig. 1. When a pH-value of 1.25 is reached, BT conversion starts to decline rapidly. Below a pH-value of 1.1, the BT conversion linearly decreases. The change of the pH to lower values is due to the formation of sulfuric acid accompanied by other organic acids, which possibly inhibit the catalyst [38] (Tab. 1 and Fig. S8).

Besides sulfur-containing acidic products, organic acids, i.e., formic acid (FA), acetic acid (AA), and oxalic acid (OA), are simultaneously formed right from the beginning of the reaction (see Figs. S8a and S8b). However, unlike FA and AA, OA is consumed during the reaction by the HPA-5 catalyst yielding CO_2, CO, and water. Thereby, HPA-5 is partly reduced, i.e., vanadium(IV) is formed (Eq. (4)). The degradation of OA can be expressed as follows:

$$\mathrm{HPA{-}5_{ox.}} + \mathrm{HOOC-COOH} \rightarrow \mathrm{HPA{-}5_{red.}} + \mathrm{CO_2} + \mathrm{CO} + \mathrm{H_2O} \quad (4)$$

This leads to an autocatalytic system, since only the reduced catalyst is able to catalyze the reaction. The O_2 molecule can only bind at the vanadium(IV) atom. As shown in Figs. S9 and S10, CO_2 as well as CO are degradation products of OA. Both compounds appear right after the concentration of OA reaches its maximum and their presence declines, when the concentration of OA drops almost to zero. If CO_2 and CO were only formed due to degradation of oxalic acid, both substrates should be detected in equal amount. However, the amount of CO_2 exceeds the content of carbon monoxide by far, and thus CO_2 must also be generated from other intermediates occurring in the oxidation path of BT.

Formic acid is the main sulfur-free product in the aqueous catalyst phase (see Fig. S8a), whereas CO_2 is the main product in the gaseous phase (see Fig. S9). Since the formic acid concentration rises during the desulfurization process, FA is only oxidized negligibly by HPA-5 to CO and water. Hence, CO is only a minor byproduct in the gaseous phase (Fig. S9).

From the concentration of all products occurring in the reaction (see Figs. S8 and S9), a carbon and sulfur mass balance was obtained, as displayed in Fig. 3. For detailed mass balances, see Figs. S11–S13. For the sulfur balance, BT, SA, SBA, and SAA, and for the carbon balance, BT, AA, FA, OA, SBA, SAA, CO, and CO_2 were taken into account.

Within the first 150 min, the total mass of sulfur found in the aqueous and organic phase reduces from 100 % to about 90 % with regard to the initial mass of sulfur. For the remaining time of the experiment, continuously 90 % of sulfur can be found. Hence, it can be assumed that a sulfur compound arises

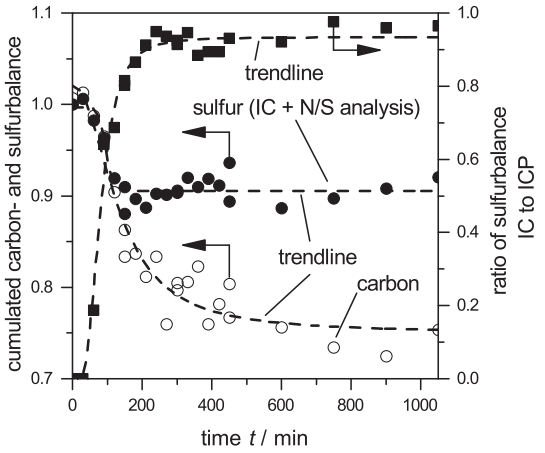

Figure 3. Mass balance of carbon and sulfur as a function of time *t* for the standard experiment. The square symbols indicate the ratio of the total mass balance of sulfur, calculated from IC, to the total mass balance of sulfur, calculated from ICP. For reaction conditions see Fig. 1.

during period II, which was not detected with the analytics used. After the first run ($t = 0$–2.5 h) ended, the reactor was opened and a brownish solid appeared. According to Khenkin und Neumann [27], heteroaromatic thiophenes, such as benzothiophene, are polymerized by a heterogeneous HPA-2 catalyst, what might also happen during the reaction under investigation. ICP analysis showed that this brownish solid contained sulfur. This precipitate is, however, not the reason for the 10 % difference in the sulfur balance alone, since its mass is too low. However, the total amount of solid could not be determined accurately, as it was unevenly spread over the entire reaction vessel. Since the solid was dispersed within the organic phase and located at the reactor wall, exact weighing was impossible. After 1050 min, the amount of that solid decreased observably, showing that the solid was slowly degrading during the reaction, corresponding to the slight linear increase of the sulfur balance.

Fig. 3 also displays the sulfur balance, characterized by the ratio of the total amount of sulfur detected in the aqueous phase by IC and the amount detected by ICP. With ICP, the total amount of sulfur in the aqueous phase was determined, whereas with IC only ionic (sulfur) products were identified. The ratio increased during the first 150 min running time, indicating that at the beginning of the reaction BT is partly oxidized to sulfur-containing products, which are soluble in water, but not of ionic character. With ongoing time, these products were further oxidized to SAA, SBA, and SA, respectively, and the ratio of sulfur balance approached a value of almost 1.

As the reaction proceeds, the carbon mass balance (Fig. 3) continuously decreased, leading to values of about 70 %. This loss of carbon was mainly due to losses of the gaseous phase, when samples were taken, since probing was carried out with syringes and losses cannot be forestalled.

 © 2020 The Authors. Published by WILEY-VCH Verlag GmbH & Co. KGaA.

3.3 Mass Transfer

In biphasic reactions, the catalyst and the substrates are present in different phases, neglecting the solid phase of the BT-polymer. Thus, the mass transport of the reactants to the catalyst is a crucial step. In the AEODS process, the mixture consists of three different phases (see Sect. 3.2):

Phase I: gaseous phase with O_2

Phase II: organic phase with BT

Phase III: aqueous phase with HPA-5

In general, the reaction can take place:

(I) In the organic phase, i.e., aqueous HPA-5 and O_2 migrate into the organic phase.

(II) At the phase boundary of the organic and aqueous phase.

(III) In the aqueous phase, i.e., BT and O_2 migrate into the aqueous phase.

In order to determine, which option is the most likely one, the volumes of both phases were varied in a series of experiments. The results are presented in Fig. 4.

The induction period decreases from 100 min to ca. 45 min, when the volume ratio $V_{aq.}/V_{org.}$ was changed from 1:1 (aqueous to organic phase) to 5:1. For the experimental series, the volume of the aqueous phase was kept constant and the volume of the organic phase was adjusted. By keeping the concentrations for HPA-5 and BT constant for all experiments, the molar sulfur-to-catalyst ratio (S/C ratio) was reduced from 100 for a volume ratio of 1:1 to 20 for a ratio of 5:1, explaining that trend. However, the sulfur-to-catalyst ratio with regard to the concentration of sulfur in the organic and HPA-5 in the aqueous phase was kept constant at 100.

The reaction rate r with regard to the organic phase enhanced with an increasing V_{aq}/V_{org} ratio, whereas the reaction rate r concerning the aqueous phase remained nearly constant. This suggests that the reaction does no take place in the organic phase, because otherwise the reaction rate r with respect to the organic phase volume should remain constant. However, the reaction rate r with regard to the aqueous phase was constant, irrespective of the volume ratio. This can be rationalized in the following way: benzothiophene migrates into the aqueous phase according to the distribution coefficient K_n to the same degree, leading to the same concentration of benzothiophene in the aqueous phase for all volume variation experiments. Given that the initial concentration of benzothiophene as well as the concentration of HPA-5 are the same in the aqueous phase in any case, the reaction rate with respect to the aqueous phase volume remains constant. Thus, the reaction takes place in the aqueous phase.

Fig. 5 illustrates the possible mass transport routes between the three phases schematically.

In order to determine the intrinsic kinetics, mass transport limitations of BT and O_2 to the aqueous phase must be excluded (see Fig. 5). Therefore, experiments were conducted, investigating the influence of stirring speed n and temperature T on the reaction.

In a series of experiments, the stirring speed was changed from 1000 min^{-1} to 1500 min^{-1}. However, the reaction rate was unaffected, i.e., the reaction rate r was found to be independent of the stirring speed (see Fig. S14). Thus, a stirring speed of 1000 min^{-1} provided a sufficient exchange surface area allowing determining the intrinsic reaction kinetics.

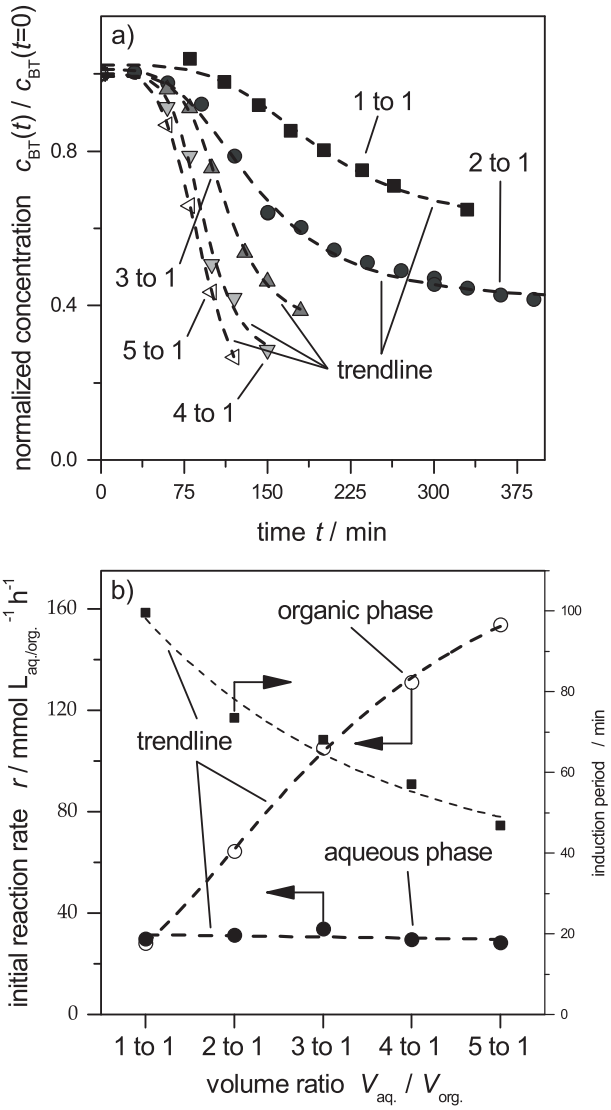

Figure 4. (a) Concentration of BT in the organic phase as function of time t for different aqueous to organic volume ratios. (b) Reaction rates r with regard to volume of aqueous and organic phase, respectively, and induction period as function of volume ratios. For reaction conditions see Fig. 1.

Variation of temperature also gives valid information, whether a reaction is mass transport-limited or not. Therefore, the temperature was varied between 90 °C and 130 °C. The results are displayed in Fig. 6 in terms of an Arrhenius plot. From this data the activation energy E_A was determined.

In the temperature range investigated, $\ln k_{eff.,aq.}$ depends linearly on T^{-1}, indicating that no mass transfer limitation occurs. The activation energy E_A was determined to be 90 ± 8 kJ mol^{-1}, which is significantly higher than for EODS with H_2O_2 as oxidant. Rezvani et al. calculated an activation energy of 52 kJ mol^{-1} for biphasic oxidation of BT with a hybrid nanocatalyst and peroxyacetic acid as oxidant [39]. This might be due to the fact that, compared to H_2O_2, oxygen has a lower oxidizing power (1.23 V for O_2 and 1.78 V for H_2O_2 vs. standard hydrogen electrode (SHE) [25]) and a higher activation barrier.

 © 2020 The Authors. Published by WILEY-VCH Verlag GmbH & Co. KGaA.

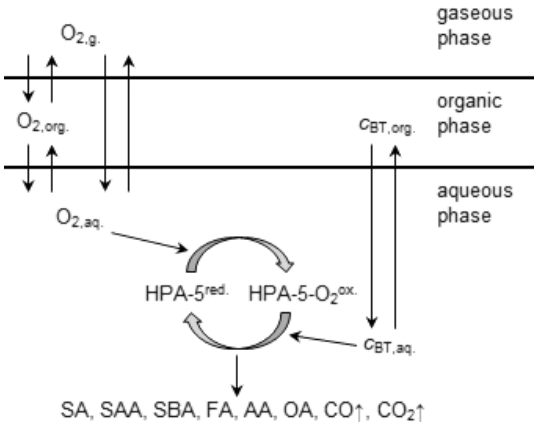

Figure 5. Scheme of phases and mass transport during an AEODS of BT with HPA-5 and O_2.

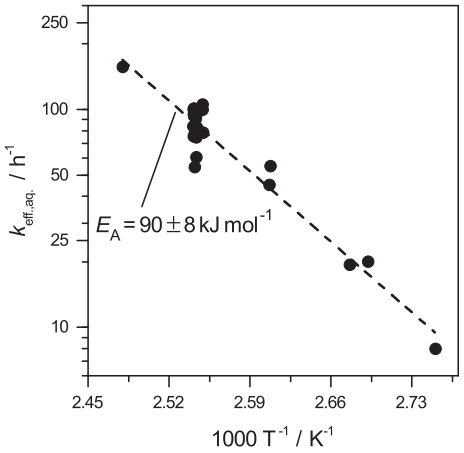

Figure 6. Arrhenius plot of $k_{eff.,aq.}$ (Eq. (5)) with K_n from Eq. (6). For reaction conditions see Fig. 1.

Since the oxygen partial pressure can be regarded as constant (see Fig. S9) at the beginning of the reaction, a pseudo first-order equation for BT was assumed (Eq. (5)).

$$r = k_{eff.,aq} c_{BT,aq} = k_{eff.,aq} K_n c_{BT,org} \quad (5)$$

As the reaction takes place in the aqueous phase, the concentration of BT in this phase has to be used for modeling. However, the concentration of BT can only be measured accurately in the organic phase. Thus, a dimensionless partition coefficient K_n was experimentally determined and the following temperature dependency was found (see Fig. S15), which sufficiently describes the amount of BT, found in the aqueous phase and is therefore used for this simple model. Here, ϑ is the temperature in °C:

$$K_n = 1.15 \times 10^{-5\,°C^{-1}} \vartheta + 2.59 \times 10^{-4} \quad (6)$$

3.4 Intrinsic Kinetics Modeled by a Power Law

In order to model the reaction rate r and hence the conversion X_{BT} of BT with HPA-5 as a catalyst and O_2 as an oxidant, the following power law kinetic approach was applied:

$$r = k_0 \exp\left(-\frac{E_A}{RT}\right) K_n c_{BT,org}^{l} c_{HPA-5}^{m} p_{O_2}^{q} \quad (7)$$

Herein, l, m and q are the reaction orders of BT, HPA-5, and O_2, respectively. $K_n c_{BT,org}$ represents the concentration of BT in the aqueous phase (compare with Eq. (5)) and k_0 is the pre-exponential factor (numerically obtained from Eq. (7)).

For the individual reaction orders of BT, HPA-5, and O_2, Eq. (7) was used in the logarithmic form and each reaction order was subsequently determined by plotting $\ln r$ over $\ln c_{BT,aq.}$, $\ln c_{HPA-5}$, and $\ln p_{oxy.}$, respectively (see Figs. S16 to S18). Tab. 2 summarizes the results.

Table 2. Values of the kinetic parameters of the power law model (Eq. (7)).

Parameter	Value in the model	Ref.
E_A	90 ± 8 kJ mol^{-1}	Eq. (5)
$k_{eff.,aq}$	7.24×10^{13} h^{-1}	Eq. (5)
k_0	1.59×10^{13} (mmol$_{HPA-5}$L$_{aq}^{-1}$)$^{0.5}$bar$^{0.5}$h^{-1}	Eq. (7)
l	1	Eq. (7)
m and q	0.5	Eq. (7)

Reaction orders for BT and O_2 are 1.22 and 0.59, respectively (see Figs. S16 and S18). However, as reaction rate data deviate by about ± 30 % (see Figs. 7a and S16–S18), the reaction orders were set to 1.0 for BT and 0.5 for O_2. In addition, the reaction order of HPA-5 was found to be 0.5 experimentally. According to Bertleff et al., the active species is explained by formation of a vanadium(V) peroxo complex, bridging two adjacent vanadium(IV) atoms within the Keggin structure of one HPA-5 with one O_2 molecule from HPA-5 containing vanadium(IV) atoms [37]. The reaction order of 0.5 for both HPA-5 and O_2 indicates that the catalytically active peroxo species is not formed via a simple one-step reaction between HPA-5 and molecular oxygen. However, it is beyond this work to elucidate this reaction sequence in order to give a mechanistic view of the formation of the active species.

As neither benzothiophene sulfoxide nor benzothiophene sulfone was detected analytically, the initial oxidation of BT to the corresponding sulfone can be regarded as the slowest step in the oxidative degradation pathway of BT. However, whether the transfer of oxygen to BT or the formation of the catalytically active HPA-5 peroxo complex is the rate-determining step is still an open question.

With the parameters from Tab. 2, the initial reaction rate r could be modeled by applying Eq. (7). Hereby, the induction period I (see Fig. 1) was neglected. Fig. 7a shows the initial reaction rates as function of the starting concentration of BT in the

 © 2020 The Authors. Published by WILEY-VCH Verlag GmbH & Co. KGaA.

aqueous phase. For comparison of initial reaction rates as function of initial concentrations of HPA-5, partial pressure of O_2, and temperature, see Figs. S19–S21.

For the entire BT concentration range investigated, the power law model given in Eq. (7) describes the measured data quite accurately. This is confirmed by the parity plot in Fig. 7b as most of the data is within the ± 20 % range.

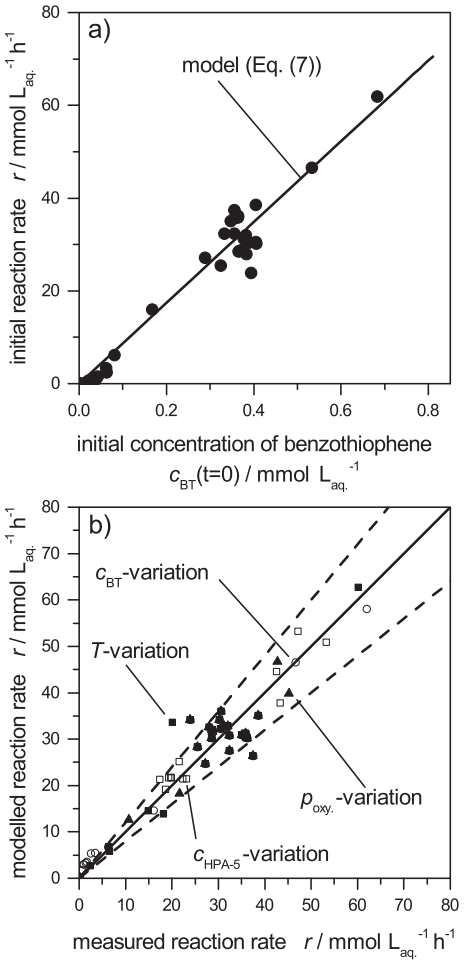

Figure 7. (a) Initial reaction rates r for varying the concentration of BT. The modeled data are depicted as solid line, based on Eq. (7) with parameters from Tab. 2. Conditions: $c_{BT,org.}(t=0)$ = 0.42 to 440 mmol $L_{org.}^{-1}$, c_{HPA-5} = 2.3 mmol $L_{aq.}^{-1}$, T = 120 °C, p_{oxy} = 17.5 bar, n = 1000 rpm. (b) Parity plot for simulation of rate r with the power law kinetic model (Eq. (7)).

With the initial rates, the BT conversion with time was calculated. In Fig. 8, the modeled and the measured conversion for the experiments with varying initial BT concentrations are given. The modeled and the measured conversion data for HPA-5 and O_2 can be found in Figs. S22 and S23.

Fig. 8b demonstrates that the conversion is satisfactorily described within the first 2.5–3 h, i.e., period II. For low BT concentrations, the model can describe the measured data only in the very early stage of the reaction. This can be explained by the fact that at low BT concentrations the vanadium(IV)

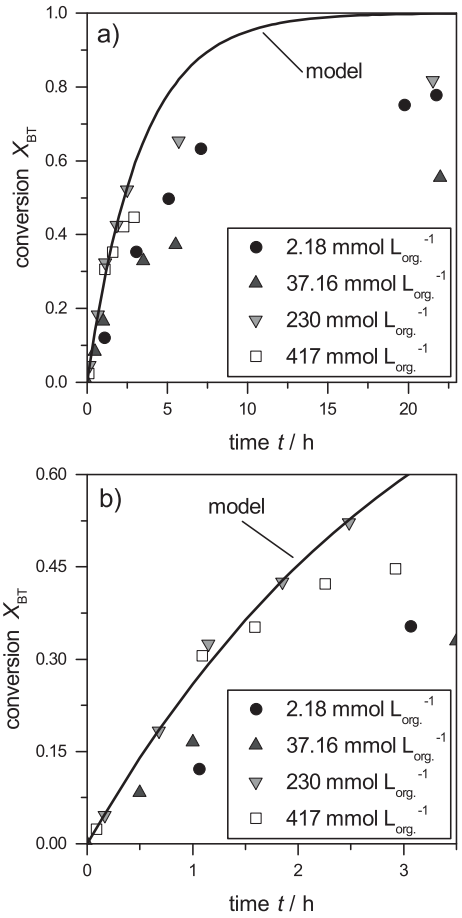

Figure 8. (a) Comparison of power law kinetic model (Eq. (7)) with experimental data for varying BT concentration. The solid line is modeled based on Eq. (7) (parameters from Tab. 2). Induction period is not shown. (b) The same data with enlarged axis. Conditions: $c_{BT,org.}(t=0)$ = 2.18 to 417 mmol $L_{org.}^{-1}$, c_{HPA-5} = 2.3 mmol $L_{aq.}^{-1}$, T = 120 °C, p_{oxy} = 17.5 bar, n = 1000 rpm.

content in HPA-5 is too low to keep the reaction running. For higher conversions (see Fig. 8b), the deviation of modeled and measured conversion is more pronounced, indicating product inhibition of HPA-5 by the acids formed in period II [38]. This is also observable in the parity plot in Fig. 9. Almost for all experiments shown, the deviation exceeds the + 20 % line for conversions > 60 %, i.e., the power law model overestimates the measured data.

4 Conclusion

Aerobic extractive oxidative desulfurization (AEODS) represents a promising catalytic approach as an alternative for hydrodesulfurization. By using oxygen as an oxidant and $H_8[PV_5Mo_7O_{40}]$ as a catalyst, benzothiophene is efficiently oxidized to water-soluble products, with sulfuric acid as the main sulfur-containing product and formic acid as the main carbon-containing product. In the gaseous phase, mainly CO_2 is found.

 © 2020 The Authors. Published by WILEY-VCH Verlag GmbH & Co. KGaA.

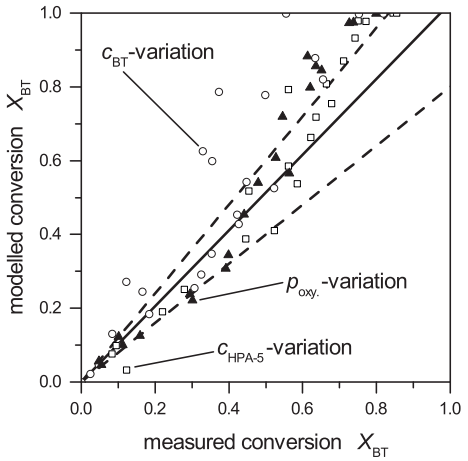

Figure 9. Parity plot of conversion X_{BT} with the power law kinetic model (Eqs. (2),(3), and (7)).

The reaction process can be divided into three different periods. Initially, the active catalyst, reduced HPA-5 with a certain amount of vanadium(IV), is formed in an induction period, taking up to 80 min. In period II, the maximum reaction rate is reached. Finally, the reaction rate declines in period III. The mass balance for sulfur and carbon is closed up to 90 % and 70 %, respectively, at any time during the reaction.

By varying the volume ratio of the aqueous to the organic phase, it appears that the reaction entirely takes place within the aqueous phase. In order to determine whether the reaction is mass transport-limited towards benzothiophene and O_2, experiments were conducted, showing no evidence of such shortcomings.

A power law kinetic model has been derived in order to model the initial reaction rate and conversion. Consequently, the concentration of benzothiophene in the aqueous phase was estimated with an experimentally determined partition coefficient within the model. The reaction orders of BT, HPA-5, and O_2 have been calculated to be 1, 0.5, and 0.5, respectively. While the initial rate is modeled satisfactorily, the conversion can only be modeled up to 60 %. At even higher conversions, product inhibition of the catalyst starts to set in. Consequently, all acidic reaction products would have to be removed, in order to keep the reaction going, according to its initial kinetics.

Acknowledgment

The authors would like to thank the Deutsche Forschungsgemeinschaft (DFG, German research foundation) for financial support within the projects JE 257/20-1 and WA 1615/14-1, Dr. Ulrike Lacher (University of Bayreuth, Germany) for ^{31}P-NMR measurements, Magdalena Wandinger for conducting experiments of the kinetic measurements, and Sabrina Hirmer for measuring the partition coefficient of benzothiophene in water/2,2,4-trimethylpentane.

The authors have declared no conflict of interest.

Symbols used

c	[mmol L^{-1}]	concentration
E_A	[kJ mol^{-1}K^{-1}]	activation energy
$k_{eff.,aq.}$	[h^{-1}]	reaction rate constant in aqueous phase
k_0	[(mmol$_{HPA-5}$L$_{aq.}$)$^{0.5}$bar$^{0.5}$h^{-1}]	pre-exponential factor
K_n	[–]	partition coefficient
l	[–]	reaction order of BT
m	[–]	reaction order of HPA-5
M	[g mol^{-1}]	molar mass
n	[mmol]	molar amount
n	[min^{-1}]	stirring rate
p	[bar]	partial pressure
q	[–]	reaction order of O_2
r	[mmol L^{-1}h^{-1}]	reaction rate
S	[–]	selectivity
t	[h]	time
T	[K]	temperature
V	[mL]	volume
V	[mL]	volume
w	[ppmw]	mass fraction
X	[–]	conversion
Y	[–]	yield

Greek letters

ϑ	[°C]	temperature
λ	[nm]	wavelength
ν	[nm^{-1}]	wavenumber
ρ	[kg m^{-3}]	density

Sub- and superscripts

0	initial
aq.	aqueous
BT	benzothiophene
eff.	effective
HPA-5	$H_8[PV_5Mo_7O_{40}]$
i	compound *i*
org.	organic
oxy.	oxygen
S	sulfur
t	time

Abbreviations

AA	acetic acid
AEODS	aerobic extractive oxidative desulfurization
BT	benzothiophene
DBT	dibenzothiophene

 © 2020 The Authors. Published by WILEY-VCH Verlag GmbH & Co. KGaA.

EODS	extractive oxidative desulfurization
FA	formic acid
FTS	Fischer-Tropsch synthesis
GC-PFPD	gas chromatography with pulsed flame photometer detector
GC-TCD	gas chromatography with thermal conductivity detector
HC	hydrocarbon
HDS	hydrodesulfurization
HPA	heteropolyacid
IC	ion chromatography
ICP-OES	inductively coupled plasma optical emission spectroscopy
IR	infrared spectroscopy
LMCT	ligand to metal charge transfer
NMR	nuclear magnetic resonance
OA	oxalic acid
ODS	oxidative desulfurization
POM	polyoxometalate
PVMo-HPA	phosphovanadomolybdo heteropolyacids
PtL	power-to-liquid
RWGS	reverse water-gas shift reaction
SA	sulfuric acid
SAA	sulfur acetic acid
SBA	2-sulfobenzoic acid
SHE	standard hydrogen electrode
T	thiophene
TG	thermogravimetry

References

[1] S. W. T. Price, D. J. Martin, A. D. Parsons, W. A. Sławiński, A. Vamvakeros, S. J. Keylock, A. M. Beale, J. F. W. Mosselmans, *Sci. Adv.* **2017**, *3 (3)*, e1602838. DOI: https://doi.org/10.1126/sciadv.1602838

[2] G. Maggio, A. Nicita, G. Squadrito, *Int. J. Hydrogen Energy* **2019**, *44 (23)*, 11371–11384. DOI: https://doi.org/10.1016/j.ijhydene.2019.03.121

[3] Y. Sun, J. He, G. Yang, V. Sage, *Catalysts* **2019**, *9 (4)*, 353. DOI: https://doi.org/10.3390/catal9040353

[4] Y. A. Daza, J. N. Kuhn, *RSC Adv.* **2016**, *6 (55)*, 49675–49691. DOI: https://doi.org/10.1039/C6RA05414E

[5] A. Varone, M. Ferrari, *Renewable Sustainable Energy Rev.* **2015**, *45*, 207–218. DOI: https://doi.org/10.1016/j.rser.2015.01.049

[6] G. Alfke, W. W. Irion, O. S. Neuwirth, in *Ullmann's Encyclopedia of Industrial Chemistry*, Wiley-VCH, Weinheim **2000**.

[7] J. G. Speight, *The Desulfurization of Heavy Oils and Residua*, 2nd ed., Chemical Industries, Vol. 78, Marcel Dekker, New York **2000**.

[8] *Thermodynamik* (Eds: H. D. Baehr, S. Kabelac), Springer, Berlin **2012**.

[9] H. Kan, C.-M. Wong, N. Vichit-Vadakan, Z. Qian, *Environ. Res.* **2010**, *110 (3)*, 258–264. DOI: https://doi.org/10.1016/J.ENVRES.2010.01.006

[10] K. Reif, *Abgastechnik für Verbrennungsmotoren*, Bosch Fachinformation Automobil, Springer, Vieweg, Wiesbaden **2015**.

[11] Richtlinie 2003/17/EG des Europäischen Parlaments und des Rates vom 3. März 2003 zur Änderung der Richtlinie 98/70/EG über die Qualität von Otto- und Dieselkraftstoffen: *Richtlinie 2003/17/EG*, Vol. 46, Europäische Union, Brüssel **2003**.

[12] *Hydrodesulfurization and Hydrodenitrogenation: Chemistry and Engineering* (Eds: T. Kabe, A. Ishihara, W. Qian), Wiley-VCH, Weinheim **1999**.

[13] A. Tanimu, K. Alhooshani, *Energy Fuels* **2019**, *33 (4)*, 2810–2838. DOI: https://doi.org/10.1021/acs.energyfuels.9b00354

[14] B. Schreiner, *Chem. unserer Zeit* **2008**, *42 (6)*, 378–392. DOI: https://doi.org/10.1002/ciuz.200800461

[15] *Ullmann's Encyclopedia, Industrial Inorganic Chemicals and Products*, Vol. 6, Wiley-VCH, Weinheim **1999**.

[16] *Chemical Technology: An Integral Textbook* (Eds: A. Jess, P. Wasserscheid), Wiley-VCH, Weinheim **2013**.

[17] J. M. Campos-Martin, M. C. Capel-Sanchez, P. Perez-Presas, J. L. G. Fierro, *J. Chem. Technol. Biotechnol.* **2010**, *85 (7)*, 879–890. DOI: https://doi.org/10.1002/jctb.2371

[18] L. Sun, T. Su, P. Li, J. Xu, N. Chen, W. Liao, C. Deng, W. Ren, H. Lü, *Catal. Lett.* **2019**, *149 (7)*, 1888–1893. DOI: https://doi.org/10.1007/s10562-019-02791-x

[19] L. Sun, T. Su, J. Xu, D. Hao, W. Liao, Y. Zhao, W. Ren, C. Deng, H. Lü, *Green Chem.* **2019**, *21 (10)*, 2629–2634. DOI: https://doi.org/10.1039/C8GC03941K

[20] Z. Ismagilov, S. Yashnik, M. Kerzhentsev, V. Parmon, A. Bourane, F. M. Al-Shahrani, A. A. Hajji, O. R. Koseoglu, *Catal. Rev.* **2011**, *53 (3)*, 199–255. DOI: https://doi.org/10.1080/01614940.2011.596426

[21] T. Hirai, K. Ogawa, I. Komasawa, *Ind. Eng. Chem. Res.* **1996**, *35 (2)*, 586–589.

[22] P. Blanc, C. Madic, J. P. Launay, *Inorg. Chem.* **1982**, *21 (8)*, 2923–2928. DOI: https://doi.org/10.1021/ic00138a003

[23] Q. Chen, C. Shen, L. He, *Acta Crystallogr., Sect. C: Cryst. Struct. Chem.* **2018**, *74 (Pt 11)*, 1182–1201. DOI: https://doi.org/10.1107/S2053229618010902

[24] I. Kozhevnikov, *Catalysis by Polyoxometalates, Catalysts for Fine Chemical Synthesis*, Vol. 2, Wiley, Chichester **2002**.

[25] F. S. Mjalli, O. U. Ahmed, T. Al-Wahaibi, Y. Al-Wahaibi, I. M. AlNashef, *Rev. Chem. Eng.* **2014**, *30 (4)*, 337–378. DOI: https://doi.org/10.1515/revce-2014-0001

[26] A. M. Khenkin, G. Leitus, R. Neumann, *J. Am. Chem. Soc.* **2010**, *132 (33)*, 11446–11448. DOI: https://doi.org/10.1021/ja105183w

[27] A. M. Khenkin, R. Neumann, *ChemSusChem* **2011**, *4 (3)*, 346–348. DOI: https://doi.org/10.1002/cssc.201000402

[28] B. Bertleff, J. Claußnitzer, W. Korth, P. Wasserscheid, A. Jess, J. Albert, *ACS Sustainable Chem. Eng.* **2017**, *5 (5)*, 4110–4118. DOI: https://doi.org/10.1021/acssuschemeng.7b00087

[29] V. F. Odyakov, E. G. Zhizhina, *React. Kinet. Catal. Lett.* **2008**, *95 (1)*, 21–28. DOI: https://doi.org/10.1007/s11144-008-5374-7

[30] C.-T. Liu, W. T. Lindsay, *J. Chem. Eng. Data* **1970**, *15 (4)*, 510–513. DOI: https://doi.org/10.1021/je60047a015

[31] W. B. Kay, F. M. Warzel, *Ind. Eng. Chem.* **1951**, *43 (5)*, 1150–1152. DOI: https://doi.org/10.1021/ie50497a044

[32] H. Salavati, N. Rasouli, *Mater. Res. Bull.* **2011**, *46 (11)*, 1853–1859. DOI: https://doi.org/10.1016/j.materresbull.2011.07.037

 © 2020 The Authors. Published by WILEY-VCH Verlag GmbH & Co. KGaA.

[33] J. Albert, D. Lüders, A. Bösmann, D. M. Guldi, P. Wasserscheid, *Green Chem.* **2014**, *16 (1)*, 226–237. DOI: https://doi.org/10.1039/c3gc41320a
[34] S. Boudjema, H. Rabah, A. Choukchou-Braham, *Acta Phys. Pol. A* **2017**, *132 (3)*, 469–472. DOI: https://doi.org/10.12693/APhysPolA.132.469
[35] H.-G. Jerschkewitz, E. Alsdorf, H. Fichtner, W. Hanke, K. Jancke, G. Öhlmann, Z. Anorg, *Allg. Chem.* **1985**, *526 (7)*, 73–85. DOI: https://doi.org/10.1002/zaac.19855260711
[36] A. Selling, I. Andersson, J. H. Grate, L. Pettersson, *Eur. J. Inorg. Chem.* **2000**, *7*, 1509–1521. DOI: https://doi.org/10.1002/1099-0682(200007)2000:7<1509:AID-EJIC1509>3.0.CO;2-7
[37] B. Bertleff, J. Claußnitzer, W. Korth, P. Wasserscheid, A. Jess, J. Albert, *Energy Fuels* **2018**, *32 (8)*, 8683–8688. DOI: https://doi.org/10.1021/acs.energyfuels.8b01514
[38] B. Bertleff, R. Goebel, J. Claußnitzer, W. Korth, M. Skiborowski, P. Wasserscheid, A. Jess, J. Albert, *ChemCatChem* **2018**, *10 (20)*, 4602–4609. DOI: https://doi.org/10.1002/cctc.201801081
[39] M. A. Rezvani, Z. Maleki, *Appl. Organomet. Chem.* **2019**, *33 (5)*, e4895. DOI: https://doi.org/10.1002/aoc.4895
[40] Verein Deutscher Ingenieure, *VDI-Wärmeatlas*, Springer, Berlin **2002**.

 © 2020 The Authors. Published by WILEY-VCH Verlag GmbH & Co. KGaA.